Submitted to the Annals of Applied Statistics
2017 Vol. , No. ,
arXiv: arXiv:0000.0000

SUPPLEMENT C: INFERENCE OF THE MICROSCOPE PARAMETERS

By Jan-Otto Hooghoudt and Rasmus Waagepetersen

In this supplementary material to "Towards Bayesian Inference of the Spatial Distribution of Proteins from Three-Cube FRET Data" we present a detailed account of the results we have obtained concerning inference of the microscope parameters, when each parameter is singly introduced as a free parameter in the model. In Section 1 we state the approach and applied settings and subsequently we discuss inference of σ^2 in Section 2, G_D and G_A in Section 3, M_D in Section 4 and of G and K in Section 5.

In order to explain many of the results, we often will refer to the equations for μ^i_{DD}, μ^i_{DA} and μ^i_{AA} as defined previously in the main article. Therefore these relations are restated here with an equation number for easy referencing throughout this supplementary material:

$$\mu^i_{DD} = M_D \sum_{d \in \mathbf{X}_D \cap C_i} (1 - P_{dA}), \tag{1}$$

$$\mu^i_{DA} = G M_D \sum_{a \in \mathbf{X}_A \cap C_i} \sum_{d \in \mathbf{X}_D} P_{da}, \tag{2}$$

$$\mu^i_{AA} = M_D / K \; n(\mathbf{X}_A \cap C_i). \tag{3}$$

Throughout this supplementary material we refer to a point pattern type by its *point pattern name* or *number* as defined in Table 1 in the main article.

1. Approach and settings. By including the microscope parameters in the Bayesian inference the joint posterior distribution—equation 3.1 in the main article—reads as

$$p(\mathbf{x}_D, \mathbf{x}_A, \theta, \psi | y) \propto p(y | \mathbf{x}_D, \mathbf{x}_A, \psi) p(\mathbf{x}_D, \mathbf{x}_A | \theta) p(\theta) p(\psi), \tag{4}$$

with $p(\psi)$ the prior density of the miscroscope parameters. The support of the microscope parameters is on $\mathbb{R}^+$ and therefore a natural choice for the proposal distribution for a microscope parameter ω_j is the lognormal distribution, which ensures that a proposal value $\omega_j^{\mathbf{p}}$ is strictly positive. Denoting by $\phi(z, \mu, \sigma^2)$ the density function of a normally distributed variable z with mean μ and standard deviation σ, the proposal density function for

$\omega_j^{\mathbf{p}}$ conditionally under its current value $\omega_j^{\mathbf{c}}$ is

$$q(\omega_j^{\mathbf{p}}|\omega_j^{\mathbf{c}}) = \frac{1}{\omega_j^{\mathbf{p}}}\phi(\ln[\omega_j^{\mathbf{p}}] \mid \ln[\omega_j^{\mathbf{c}}], \tau_j^2),$$

with τ_j^2 a tuning parameter, controlling the percentage of accepted proposals within a MCMC run. A proposal $\omega_j^{\mathbf{p}}$ is now generated by drawing a random normal number $\epsilon \sim N(0, \tau_j^2)$ and setting $\omega_j^{\mathbf{p}} = \omega_j^{\mathbf{c}} \exp(\epsilon)$. We note that as $\phi(\cdot)$ is symmetric around its mean it follows that

$$\frac{q(\omega_j^{\mathbf{c}}|\omega_j^{\mathbf{p}})}{q(\omega_j^{\mathbf{p}}|\omega_j^{\mathbf{c}})} = \frac{\omega_j^{\mathbf{p}}}{\omega_j^{\mathbf{c}}}.$$

Applying (4), the Metropolis-Hastings ratio related to a proposal $u \sim q_j(\cdot|\omega_j^{\mathbf{c}})$ for the j-th microscopic parameter is

$$\left(\frac{p(y|\psi^{\mathbf{p}}, \mathbf{x}^{\mathbf{c}})}{p(y|\psi^{\mathbf{c}}, \mathbf{x}^{\mathbf{c}})}\right) \left(\frac{p(\psi_j^{\mathbf{p}})}{p(\psi_j^{\mathbf{c}})}\right) \quad \left(\frac{q(\psi_j^{\mathbf{c}}|\psi_j^{\mathbf{p}})}{q(\psi_j^{\mathbf{p}}|\psi_j^{\mathbf{c}})}\right), \tag{5}$$

with $\psi^{\mathbf{c}} = (\omega_1^{\mathbf{c}}, \cdots, \omega_6^{\mathbf{c}})$ containing the current values for the microscope parameters and $\psi^{\mathbf{p}}$ containing the elements

$$\psi_k^{\mathbf{p}} = \begin{cases} \omega_j^{\mathbf{c}} & k \neq j \\ u & k = j. \end{cases}$$

The expressions for the first two terms in (5) are specified under step 10 in Section 1 of Supplement B (Hooghoudt and Waagepetersen, 2017) while the third term equals $\omega_j^{\mathbf{p}}/\omega_j^{\mathbf{c}}$. Supplement B provides a detailed description of the MCMC sampler used for sampling from the posterior distribution (4).

1.1. *Set up of the various simulation experiments.* Below we give a short description of each of the simulations that have been carried out and state the settings that have been used. In order to study the effect a relatively low or high signal-to-noise ratio has on the inference, each simulation has been performed for three synthetic values of M_D $(1, 5, 20)$. In the next we denote the prior mean of a parameter by adding the superscript "pm" to the parameter.

A All microscope parameters are fixed in the inference procedure (the MCMC run) and set to the values of their synthetic counterparts applied to create the synthetic channel data. The synthetic value of the parameters G, K, G_D, G_A is set to 1 and the synthetic value of σ^2 is

set to 25. Synthetic channel data is generated for a grid $\mathbf{G}$ which divides the window $W = 1 \times 1 \mu\text{m}^2$ in 10×10 equally sized square pixels. Accordingly the dimension of a pixel is 0.1×0.1 μm^2. The Poisson point process intensities θ_D and θ_A are free parameters and their prior means are set approximately equal to the intensities of the synthetic patterns, i.e. $\theta_D^{\text{pm}} = \theta_A^{\text{pm}} = 1000/\mu\text{m}^2$. In this simulation, inference is made on the spatial configuration of donors and acceptors and on the Poisson point process intensities θ_D and θ_A. Interest is in assessing how the accuracy of the posterior L-function depends on the underlying point pattern type. The outcomes of Simulation A are disussed in the main article in Section 4.3 and its subsections.

B Settings as in Simulation A, but σ^2 is a free parameter. The prior mean value of σ^2 is set equal to the synthetic value of 25. Interest is in studying the inference for the parameter σ^2. Results are discussed in Section 2.

C-G Settings as in Simulation A, but G_A, G_D, M_D, G, K are respectively (each separately) a free parameter in the model. Prior mean of the free parameter is always set equal to the synthetic value of 1. Results for G_A and G_D are discussed in Section 3, for M_D in Section 4 and for G and K in Section 5.

H Settings as in Simulation A, but $M_D, G, K, G_D, G_A, \sigma^2$ are free parameters with their prior means set equal to the corresponding synthetic values. Interest is in studying the inference of all the microscope parameters in the setting that they are all free. Results are discussed in Section 4.4 in the main article.

In Table 1 the settings of each of the simulations are summarized.

1.2. *Hyper parameters of the priors.* The Gamma distribution is used as the prior density for the microscope parameters. Following the reasoning as outlined for setting the Poisson priors in Section 3.1 in the main article, we also set the shape parameter of the microscope parameters equal to 4. In our simulations we specify the prior mean of each of the microscope parameters (see Table 1). Then, if the value of the mean is denoted m the scale parameter β follows from $\beta = m/\alpha = m/4$.

1.3. *Markov chain Monte Carlo settings.* The total number of steps in each MCMC run is set to 1e7. A proposal update is made in each step to remove/add a donor or acceptor point to/from the current point pattern. A posterior point pattern is written to disk after every 1e5 steps. A proposal update for the microscope parameters (in case free) and for the Poisson point

	Within the MCMC run						Synthetic value					
Simulation	M_D	G	K	G_D	G_A	σ^2	M_D	G	K	G_D	G_A	σ^2
A	$\star$	$\star$	$\star$	$\star$	$\star$	$\star$	1,5,20	1	1	1	1	25
B	$\star$	$\star$	$\star$	$\star$	$\star$	F	1,5,20	1	1	1	1	25
C	$\star$	$\star$	$\star$	$\star$	F	$\star$	1,5,20	1	1	1	1	0.1
D	$\star$	$\star$	$\star$	F	$\star$	$\star$	1,5,20	1	1	1	1	0.1
E	$\star$	$\star$	F	$\star$	$\star$	$\star$	1,5,20	1	1	1	1	0.1
F	$\star$	F	$\star$	$\star$	$\star$	$\star$	1,5,20	1	1	1	1	0.1
G	F	$\star$	$\star$	$\star$	$\star$	$\star$	1,5,20	1	1	1	1	0.1
H	F	F	F	F	F	F	1,5,20	1	1	1	1	25

$\star$ fixed parameter set equal to the synthetic value.
F free parameter with its prior mean equal to the synthetic value.

TABLE 1

Parameter settings as defined for the various simulations. All simulations are performed on a window $W = 1 \times 1\mu m^2$ and a grid dividing W in 10×10 square pixels with a width of 0.1 μm. In each simulation the Poisson intensities are free parameters with a prior mean value of $1000/\mu m^2$. For Simulations C–G we have set the synthetic value of σ^2 (almost) equal to zero, in order to get the most accurate inference regarding G_A, G_D, K, G and M_D as possible.

process intensities is made every 2.5e3 steps. We store the parameter and intensities values to disk every 1e4 steps. So, for each complete MCMC run, one thousand values of the microscope parameters and Poisson intensities, and one hundred point patterns are stored to disk. The initial values of the point process intensities and the free microscope parameters are always set equal to their respective prior means.

1.4. *Tuning parameters of the proposal distributions..* To generate proposals for the microscope parameters we have used the following values for the tuning parameter τ in the lognormal distribution. To generate proposals: for M_D we used $\tau = 0.04$; for G and K we used $\tau = 0.05$; and for σ^2, G_A and G_D we used $\tau = 0.1$. In all cases the applied setting result in acceptance probabilities between 0.1–0.6 depending on the value of M_D. Higher values of M_D—corresponding to a higher signal-to-noise ratio—result in lower acceptance rates.

2. Inference of the measurement noise. In Figure 1 the posterior means of the measurement noise standard deviation ($\bar{\sigma}$) for the replicated

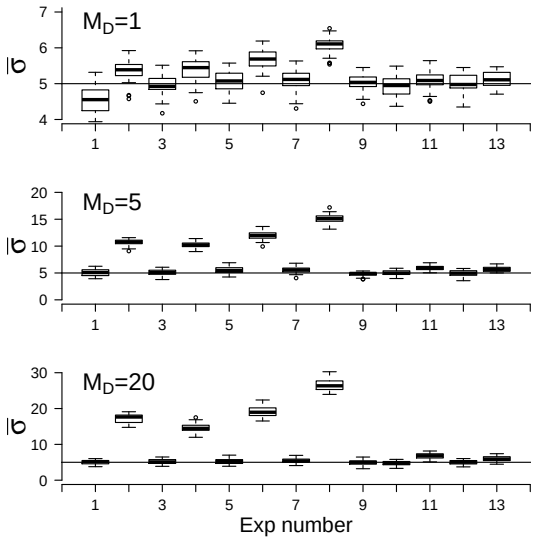

FIG 1. *Boxplot of the posterior mean measurement noise standard deviation of the forty replicated runs, for each of the point pattern types (referred to by their type number as denoted in Table 1 in the main article), for $M_D = 1$ (upper), $M_D = 5$ (middle) and $M_D = 20$ (lower). Results are from Simulation B; σ^2 is a free parameter. The horizontal lines are drawn at the synthetic value of σ which is 5.*

runs (from Simulation B) are summarized for each of the point pattern types by a boxplot. Results are shown for M_D equal to 1, 5 and 20. Clearly, the dimer and clustered point pattern types generated with $\gamma_{DA} = 8$ (type number: 2,4,6 and 8) show values for $\bar{\sigma}$ larger than the synthetic value of 5 for all three values of M_D. Further, saliently, the bias grows significantly for larger values of M_D. For all other point pattern types, $\bar{\sigma}$ is consistently close to five for all three values of M_D. We conclude that for modestly clustered point patterns (dimer and clustered types generated with $\gamma_{DA} = 2$) as well as for the Poisson and repulsive types, the inference of σ performs well. The results found for the dimer and clustered point patterns generated with $\gamma_{DA} = 8$ are surprising. We investigate this issue in the next section.

2.1. *Persistent bias in posterior DA-channel intensity.* To understand the cause of the offset between the posterior mean measurement noise standard deviation and its synthetic value we will study the posterior mean *pixel deviance*—as defined below—over replicated runs for each point pattern type, for the case that all microscope parameters are fixed to their synthetic value (that is settings as in Simulation A). We start by defining the *deviance* as used in this supplementary material. For a random variable Z,

distributed with mean μ and variance σ^2 and for which n observations have been made, we refer to the quantity $\mathrm{DEV}(Z) = (1/n)\sum_{i=1}^{n}((Z_i - \mu)/\sigma)^2$ as the deviance. By the definition of the variance: $\sigma^2 = \mathrm{E}[(Z - \mathrm{E}[Z])^2]$, the expected value of the deviance is one, that is $\mathrm{E}[\mathrm{DEV}(Z)] = 1$. Applying the deviance definition to the pixel intensities in the three channels (equations (2.1)–(2.3) in the main article), and defining n to be the number of pixels in a channel image, we define the *deviance* for each of the three channels as

$$\mathrm{DEV}_{DD} \equiv \mathrm{DEV}(Y_{DD}|\mu_{DD}) = \frac{1}{n}\sum_{i=1}^{n}\frac{(Y_{DD}^i - \mu_{DD}^i)^2}{G_D\mu_{DD}^i + \sigma^2}, \tag{6}$$

$$\mathrm{DEV}_k \equiv \mathrm{DEV}(Y_k|\mu_k) = \frac{1}{n}\sum_{i=1}^{n}\frac{(Y_k^i - \mu_k^i)^2}{G_A\mu_k^i + \sigma^2} \quad ; k = DA, AA. \tag{7}$$

In Figure 2 the posterior mean of the channel deviance for the replicated runs (results from Simulation A) are summarized by aid of a boxplot for each

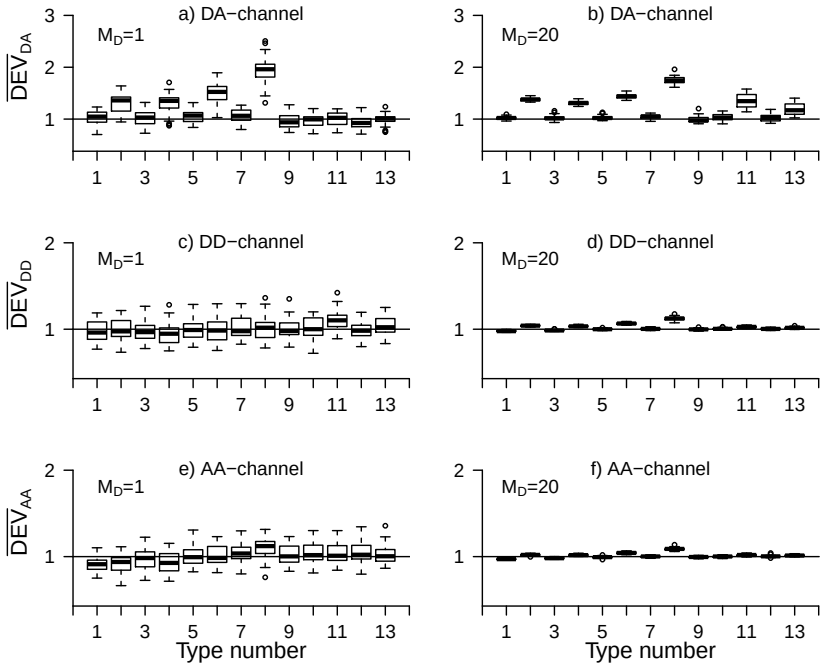

FIG 2. *Boxplot of the posterior mean deviance of the forty replicated runs for each of the point pattern types (referred to by their type number as defined in Table 1 in the main article) and for each of the three channels. Upper plots: DA-channel, middle plots: DD-channel and lower plots: AA-channel, for* $M_D = 1$ *(left figures) and* $M_D = 20$ *(right figures). Results are from Simulation A.*

of the point pattern types and each of the three channels. For $M_D = 1$ the posterior mean deviance in the DA-channel, plot a), is clearly above one for the point patterns with type number: 2, 4, 6, 8 (that is the patterns generated with a $\gamma_{DA} = 8$), while it is on the target value of one for all other types. Also for $M_D = 20$ the posterior mean deviances in the DA-channel, plot b), are persistently above one for the strongly clustered types (type number: 2, 4, 6, 8), while now also the deviance related to the strongly repulsive patterns (Rep.h2 and Rep.s2, type number 11 and 13) are slightly above target. In contrast, in the DD-channel, plot c) and d), and AA-channel, plot e) and f), the posterior mean deviance for all point pattern types are close to one for $M_D = 1$ as well as for $M_D = 20$. In short, our main observation from the various deviance plots is that for the strongly clustered and strongly repulsive point patterns, the inference procedure has—also for a high signal-to-noise ratio (high M_D)—significant problems to get on target in the DA-channel.

To study this offset in the DA-channel further Figure 3 shows the posterior mean pixel intensities $\bar{\mu}^i_k, k = DD, DA, AA$, versus the corresponding synthetic pixel intensities $Y^i_{k,\text{synth}}$ for the three values of M_D, and where $Y_{k,\text{synth}}$ is generated from a Clu.28 point pattern type. The results are from Simulation A; σ^2 is fixed and set equal to the synthetic value of 25. Clearly, the $\bar{\mu}^i_{DD}$'s and $\bar{\mu}^i_{AA}$'s get properly on target for higher values of M_D (from left to right in respectively the upper and lower plots). Also the $\bar{\mu}^i_{DA}$'s are closer to target for higher values of M_D, although for $M_D = 20$ still a persistent negative bias compared to the synthetic DA-channel pixel intensity is observed (right middle plot). Similar scatter plots for point pattern types Dim.18, Dim.28 and Clu.28, display a similar bias in the DA-channel (not shown). Scatter plots for point pattern types Rep.h2 and Rep.s2, show a positive bias in the DA-channel, that is $\bar{\mu}^i_{DA}$ is mostly larger than Y^i_{DA} (not shown). We conclude that a persistent negative (positive) bias in the posterior DA-channel pixel intensities is present when making inference on synthetic channel data constructed from strongly clustered (repulsive) point patterns.

By the previous analyses we can now explain the large offset observed in Figure 1 between the posterior means of the measurement noise standard deviation and the synthetic value. Due to the bias in the DA-intensity channel—values of DEV_{DA} larger than one—the inference procedure with σ^2 a free parameter in the model (Simulation B), will increase σ^2 in order to get DEV_{DA} on target. However, the increase in σ^2 results in a further increase in the bias of the posterior DA-pixel intensities, resulting again in a further increase of σ^2. This explanation is supported by Figure 4 in which

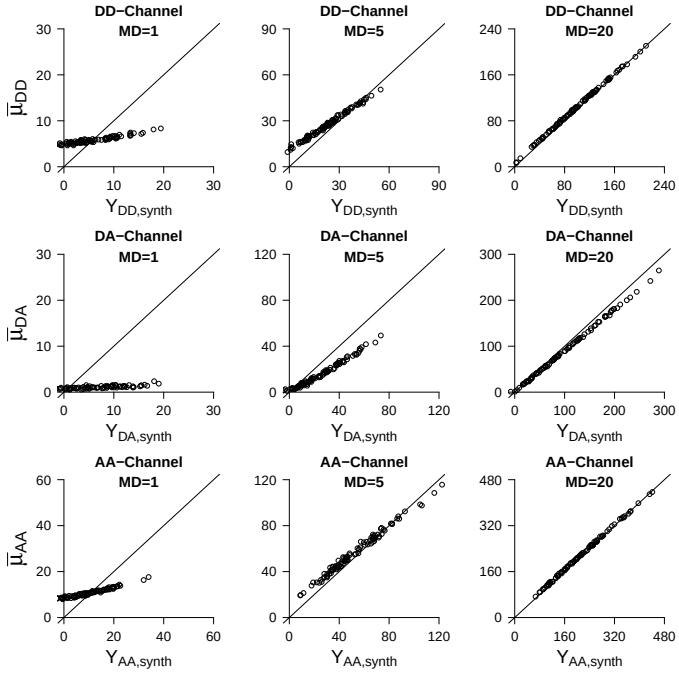

FIG 3. *Scatter plots of the posterior mean pixel intensities:* $\bar{\mu}_k^i$*, versus the corresponding synthetic pixel channel intensities* $Y_{k,synth}^i$ $k = DD, DA, AA$, $i = 1, \ldots, n$; $n = 100$. *With* $Y_{k,synth}$ *generated from a point pattern* $\mathbf{X}_{synth}$ *of Clu.28 type. From left to right:* $M_D = 1, 5, 20$*; from above to below: DD-, DA- and AA-channel. For higher values of* M_D*, the posterior mean DD- and AA-channel pixel intensities get on target, while the posterior mean DA-channel pixel intensities remain below target. Black line is reference line with slope 1.*

the posterior mean values of σ are plotted versus the corresponding synthetic pixel intensities for the same Clu.28 point pattern as the results in Figure 3 are based on, but now σ^2 is a free parameter in the model (posterior means are from Simulation B). Clearly, with σ^2 a free parameter in the model, the offset between posterior mean DA-intensity and synthetic DA-channel intensity increases (compare Figure 4 middle plots, with corresponding plots in Figure 3). Further, due to the increase in σ^2 now also the posterior mean intensities in the DD- and AA-channel have difficulty to get on target (compare Figure 4, upper and lower plots, with corresponding plots in Figure 3).

In summary, due to a relative large offset between the Poisson point process prior model and the strongly clustered and repulsive patterns, a persistent bias exist between the posterior pixel mean intensities and the synthetic

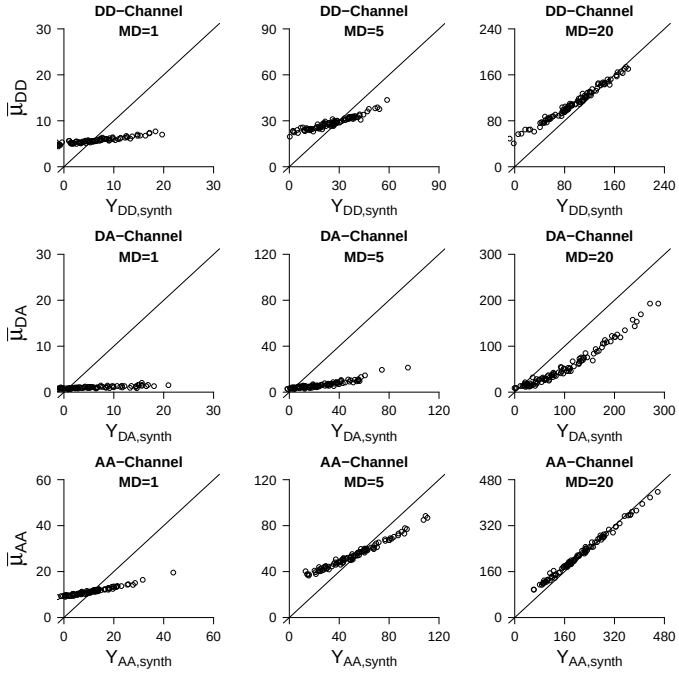

FIG 4. *As Figure 3 but results are from Simulation B; σ^2 is a free parameter. Due to the bias of the posterior mean intensity in the DA-channel—see in Figure 3—with σ^2 a free parameter the inference procedure will start to increase σ^2, which leads to a further increase in the bias in the DA-channel. Because σ^2 defines the measurement noise in all the three channels also in the DD- and AA-channel the posterior pixel intensities now have difficulties to get on target (upper and lower plots).*

pixel intensities in the DA-channel. This results in biased inference for σ.

3. Inference of the amplification factors. The results concerning inference of G_A are in accordance with the results as discussed in the previous section for the measurement noise. Due to the persistent bias in the posterior DA-channel intensities for strongly clustered patterns, for such patterns G_A is excessively increased in the inference procedure in order to get DEV_{DA} (7) on its target value of one. This is clearly seen in Figure 5 (left plots), as for the pattern types 2, 4, 6 and 8 the values of $\bar{G}_A$ are clearly above the synthetic value of one for all three values of M_D, while on target or close to target for all other point pattern types.

The parameter G_D only effects DEV_{DD} (6) and thereby G_D can not be tuned in the inference procedure to adjust DEV_{DA} (7). Therefore, we would expect that proper inference for this parameter should be possible for all point pattern types. However, from Figure 5 (right plots) we notice that

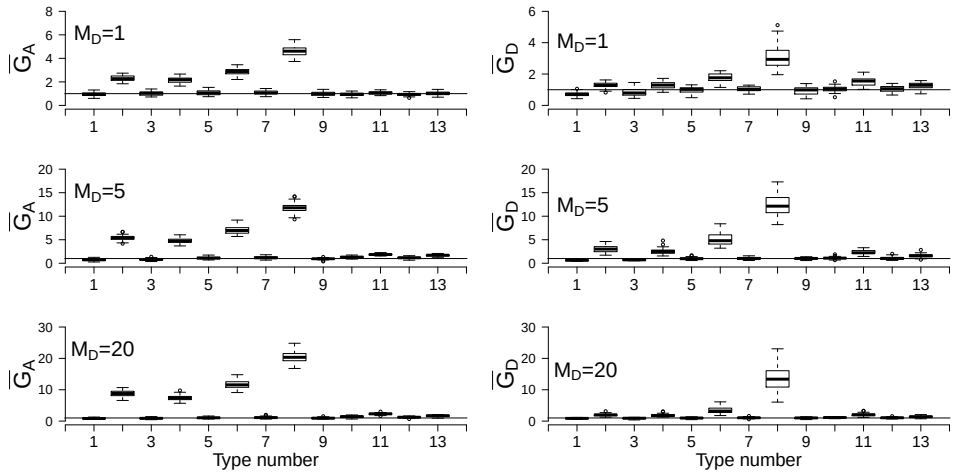

FIG 5. *Boxplots of the posterior mean of: left) G_A and right) G_D, for the forty replicated runs for each of the point pattern types (referred to by their type number as denoted in Table 1 in the main article), for $M_D = 1$ (upper), $M_D = 5$ (middle) and $M_D = 20$ (lower). The horizontal lines are drawn at the synthetic values $G_A = 1$ (left plots) and $G_D = 1$ (rigth plots).*

for the strongly clustered patterns (type 2, 4, 6, 8) also the value of $\bar{G}_D$ is above the synthetic value of one, which is most clearly seen for Clu.28 (type 8). The probable explanation is that for the strongly clustered patterns also a small but significant persistent bias exists in the DD-channel intensities, leading to values of DEV_{DD} slightly above the target value of one. This is supported by Figure 2, where especially for Clu.28 (type 8) it is rather clearly seen that DEV_{DD} is above one for $M_D = 20$.

We conclude that, except for the strongly clustered point patterns, the inference procedure provides good estimates for G_A and G_D.

4. Inference of M_D. In Figure 6 the posterior mean of M_D for the forty replicated runs is summarized by aid of a boxplot for each of the point pattern types and for $M_D = 1, 5, 20$. Results are of Simulation E. Inspection of the plots shows that there is a clear trend in the observed posterior means.

1. for underlying clustered patterns (type 1–8), the values of $\bar{M}_D$ are smaller than the corresponding synthetic values. Further, the bias is larger for the strongly clustered point patterns generated with $\gamma_{DA} = 8$ (type 2, 4, 6 and 8).[2]

[2]We ignore here for the moment the values of $\bar{M}_D$ larger than their synthetic counterparts occurring for type 8 and M_D is 5 or 20. We comment on it at the end of this

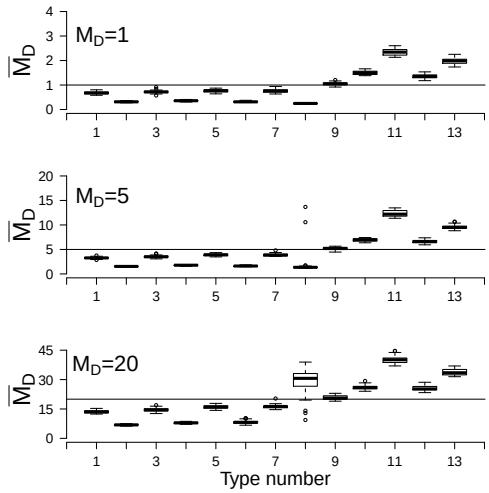

FIG 6. *Boxplot of posterior mean of M_D for the forty replicated runs for each of the point pattern types (referred to by their type number as denoted in Table 1 in the main article), for $M_D = 1$ (upper), $M_D = 5$ (middle) and $M_D = 20$ (lower). In each plot the horizontal line is drawn at the synthetic values of M_D. Results are from Simulation E.*

2. for underlying repulsive patterns (type 10–13), the values of $\bar{M}_D$ are larger than the corresponding synthetic values and the bias increases for the strongly repulsive point patterns (type 11 and 13, that is Rep.h2 and Rep.s2).
3. for underlying Poisson hard core patterns (type 9), the value of $\bar{M}_D$ coincides with the corresponding synthetic value.

Further, the observed bias for the dimer, clustered and repulsive patterns is persistent in the sense that increasing the signal-to-noise ratio (by increasing M_D) does not result in a decrease of the bias.

The bias is an artifact of the use of the Poisson point process prior. The explanation is as follows. When inference is made with all the microscope parameters fixed to their synthetic values (Simulation A) on a *strongly hetero pair clustered* point pattern, the inference procedure has difficulties to create such clusters, because the Poisson point process prior will favor a more random distribution of the hetero points. This results, as previously discussed in Section 2, in a negative bias of the posterior pixel mean DA-channel intensities, μ^i_{DA}, and of values of DEV_{DA} above the target value of one (Figures 2 and 3). To reduce the bias, the inference procedure—with M_D a free parameter (Simulation E)—favors to add more acceptors to the poste-

section.

rior pattern than the corresponding synthetic pattern contains. By adding extra acceptors, the average hetero pair inter distances decrease, resulting in an increase of the double summation term in (2)—and so of $\bar{\mu}^i_{DA}$—thereby effectively removing the bias. Increasing the number of acceptors will lead to a positive bias of μ^i_{AA} (3). However, this bias is removed by the inference procedure by decreasing the value of M_D and so getting μ^i_{AA} on target again. As M_D is also present in the expression for μ^i_{DD} (1), this leads to a bias in the DD-channel, which, however, is removed by the inference procedure by adding more donors to the posterior patterns than the underlying synthetic pattern contains, effectively getting μ^i_{DD} back on target. Further, by (2), μ^i_{DA} is also proportional to M_D and by lowering M_D also μ^i_{DA} will be lower. However, the relative increase of the double summation term in (2) due to the higher concentrations of acceptors is larger than the relative decrease of M_D, resulting in an increase of the DA-channel pixel intensities and so bringing μ^i_{DA} onto target.

The same argument holds for underlying repulsive patterns but the other way around. In this case the posterior μ^i_{DA}'s—with all microscope parameters fixed to their synthetic values— show a positive bias with respect to the synthetic channel data. And the inference procedure—with M_D a free parameter—favors posterior patterns to contain less donors and acceptors than the synthetic pattern, thereby increasing the average hetero pair inter distances and bringing the posterior pixel intensities in the DA-channel onto target. This leads to a higher value of M_D with respect to the corresponding synthetic value.

We now will discuss the in the footnote on the previous page mentioned inference results concerning the Clu.28 patterns (type 8), for which for $M_D = 5$ some, and for $M_D = 20$ most of the posterior means $\bar{M}_D$ are higher than these synthetic values. Clearly these results are not captured by the explanation stated above. They can, however, be explained in relation to the large offset that exists between the *homogeneous* Poisson point process prior and the very *inhomogeneous* way donors and acceptors are distributed over the pixels in Clu.28 patterns. We will give a qualitative description. For the clustered point patterns type 1–7, hetero clustering occurs in such a way that the donors and acceptors are more or less homogeneously distributed over the pixels. This is schematically depicted in Figure 7a, as a dimer pair residing in each of the pixels. For the point pattern types 1–7, to get the DA-channel intensities on target the posterior patterns will contain more donors and acceptors—as described in detail above— than the corresponding synthetic patterns (see, Figure 7b), resulting in posterior mean values of M_D lower

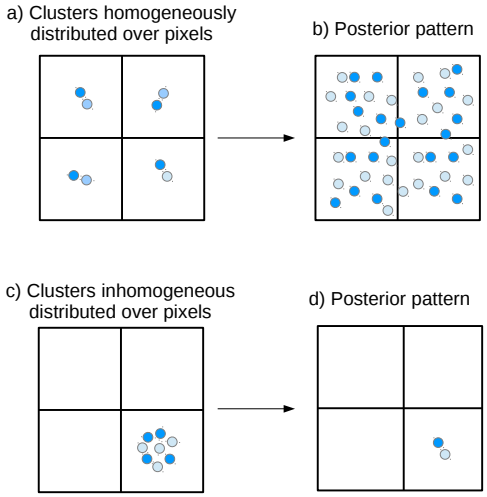

FIG 7. *Point patterns for which hetero cluster of points are distributed: a) homogeneously, and c) inhomogeneously, over the pixels. For hetero clusters distributed homogeneously over the pixels, the inference procedure—with M_D a free parameter—favors the posterior patterns to contain more donors and acceptors than the synthetic one (plot b)) and to decrease the value of M_D below the synthetic value. For hetero clusters distributed inhomogeneously over the pixels, the inference procedure favors to decrease the number of donors and acceptors (plot d)) and to increase M_D. See also the text.*

than the corresponding synthetic value. For the Clu.28 type point patterns, however, the hetero clustering is so strong that this results in large super clusters of donors and acceptors, leading to a very *inhomogeneous* distribution of donors and acceptors over the pixels. This is schematically depicted in Figure 7 c), in which all points are concentrated in only one pixel. As such a distribution is extremely unlikely to occur under the *homogeneous* Poisson point process prior, the inference procedure favors to: place only a few points in an inhomogeneous way over the pixels—which under the Poisson process prior and conditional under a fixed number of points, has a higher probability than to place many point inhomogeneously (see Figure 7 d), while using a higher value of M_D than the synthetic value, in order to get the the posterior channel intensities onto target.

We conclude that the results of the inference of M_D are highly dependent on the synthetic point pattern type.

5. Inference of the G and K factor. In Figure 8 left) the results concerning inference of G (Simulation F) are shown. Clearly, $\bar{G}$ is larger than the synthetic value of one for clustered point patterns (type numbers 1–8) while smaller than one for the repulsive point patterns (type numbers

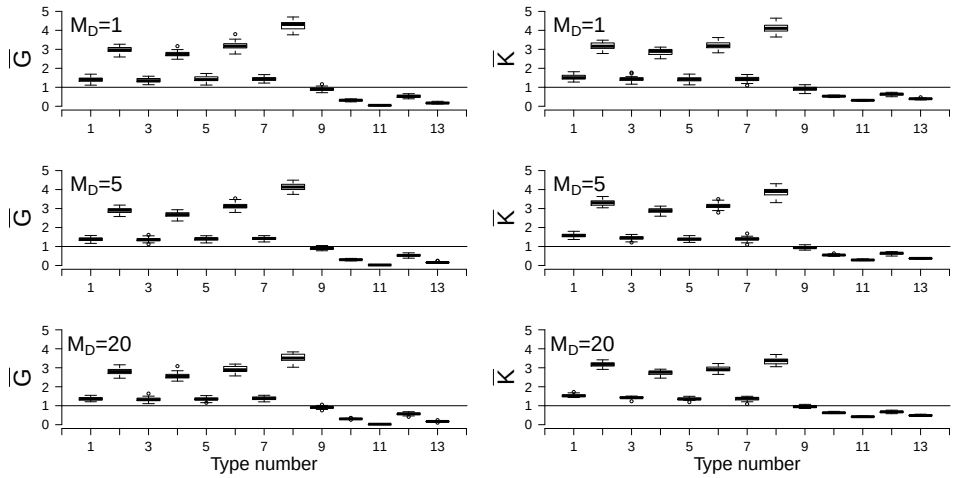

FIG 8. *Boxplot of posterior mean of: left) G, and right) K, for the forty replicated runs for each of the point pattern types (referred to by their type number as denoted in Table 1 in the main article), for $M_D = 1$ (upper plots), $M_D = 5$ (middle plots) and $M_D = 20$ (lower plots). In each plot the horizontal line is drawn at the synthetic value $G = 1$ (left plots) and the synthetic value $K = 1$ (right plots). Results of $\bar{G}$ and $\bar{K}$ are from Simulations F and G, respectively.*

10–13). Further, the offset is larger for the more strongly clustered (types 2, 4, 6, 8) and more strongly repulsive (types 11 and 13) point patterns. For underlying Poisson hard core patterns (type 9), the value of $\bar{G}$ coincides with, or is close to, the synthetic value of one. These results can again be explained by the relative offset between the prior Poison process model and the pattern types. With G a free parameter in the model, any existing consistent positive or negative bias of the posterior DA-channel pixel mean intensities—μ^i_{DA} (2)—and the corresponding synthetic data Y^i_{DA}'s can effectively be removed by the tuning of G in (2). For underlying clustered patterns, the inference procedure favors to increase G in (2)—in order to match the μ^i_{DA}'s with the Y^i_{DA}'s—instead of increasing the value of the double summation term in (2) by placing donors and acceptors sufficiently close to each other. Similar, for underlying repulsive patterns, the inference procedure favors to decrease G in (2)—in order to match the μ^i_{DA}'s with the Y^i_{DA}'s—instead of decreasing the value of the double summation term in (2) by placing donors and acceptors sufficiently far from each other.

In Figure 8 right) the results concerning inference of K (Simulation G) are shown. Clearly, $\bar{K}$ is larger/smaller than the synthetic value of one for clustered/repulsive underlying point patterns (type number 1–8 and 10–13, respectively). Further, the offset is larger for the strongly clustered (type

number 2,4,6,8) and strongly repulsive (type number 11 and 13) point patterns. For underlying Poisson hard core patterns (type 9), the value of $\bar{K}$ coincides with, or is close to, the correct value of one. With K a free parameter in the model, any existing consistent positive or negative bias of the posterior DA-channel pixel intensities can be removed by tuning the number of acceptors within the posterior patterns. For underlying clustered patterns, the inference procedure favors to increase the number of acceptors with respect to the underlying synthetic pattern. Hereby, the value of the double summation term in (2) increases, effectively removing the negative bias between the μ^i_{DA}'s and Y^i_{DA}'s. The increase in acceptors leads to an offset in the AA-channel intensities (2), but this offset is removed by increasing the value of K in (2). Similar, for underlying repulsive patterns, the inference procedure favors to remove acceptors, resulting in a smaller value of K compared to the synthetic value of one.

We conclude that the results of the inference of G and K are highly dependent on the point pattern type.

References.

Hooghoudt, J.-O. and Waagepetersen, R. (2017). Supplement B: The MCMC sampler. *Annals of Applied Statistics*.

Jan-Otto Hooghoudt
Aalborg University
Department of Civil Engineering
Aalborg, Denmark
E-mail: joh@civil.aau.dk

Rasmus Waagepetersen
Aalborg University
Department of Mathematics
Aalborg, Denmark
E-mail: rw@math.aau.dk